AIP | Applied Physics Letters

Detecting ZnSe secondary phase in Cu2ZnSnSe4 by room temperature photoluminescence

Rabie Djemour, Marina Mousel, Alex Redinger, Levent Gütay, Alexandre Crossay et al.

Citation: Appl. Phys. Lett. **102**, 222108 (2013); doi: 10.1063/1.4808384
View online: http://dx.doi.org/10.1063/1.4808384
View Table of Contents: http://apl.aip.org/resource/1/APPLAB/v102/i22
Published by the American Institute of Physics.

Detecting ZnSe secondary phase in $Cu_2ZnSnSe_4$ by room temperature photoluminescence

Rabie Djemour,[1,a)] Marina Mousel,[1] Alex Redinger,[1] Levent Gütay,[1,b)] Alexandre Crossay,[2] Diego Colombara,[2] Phillip J. Dale,[2] and Susanne Siebentritt[1]
[1]*Laboratory for Photovoltaics, University of Luxembourg, Belvaux, Luxembourg*
[2]*Laboratory for Energy Materials, University of Luxembourg, Belvaux, Luxembourg*

(Received 7 March 2013; accepted 17 May 2013; published online 7 June 2013)

Secondary phases, such as ZnSe, occur in $Cu_2ZnSnSe_4$ and can be detrimental to the resulting solar cell performance. Therefore, it is important to have simple tools to detect them. We introduce subband gap defect excitation room temperature photoluminescence of ZnSe as a practical and non-destructive method to discern the ZnSe secondary phase in the solar cell absorber. The PL is excited by the green emission of an Ar ion laser and is detected in the energy range of 1.2–1.3 eV. A clear spatial correlation with the ZnSe Raman signal confirms this attribution. © *2013 AIP Publishing LLC*. [http://dx.doi.org/10.1063/1.4808384]

$Cu_2ZnSnSe_4$ (CZTSe) is a prominent candidate absorber for future solar cell technology.[1] Pure CZTSe quaternary material is difficult to grow single phase due to a small single phase region.[2–4] The occurrence of secondary phases, potentially even within the single phase existence region, depends critically on the synthesis method. The best CZTSe solar cell absorbers are grown outside this single phase region: under Zn-rich and Cu-poor conditions (compared to stoichiometric CZTSe)[1,5] which, according to the phase diagram, would result in the presence of ZnSe and SnSe as possible secondary phases.[2]

Ideal solar cell absorbers should be single phase to prevent absorption and/or recombination losses or high series resistances as summarized in Ref. 6. Therefore, it is important to have techniques to detect the presence of the secondary phases. In this paper, we focus on the detection of ZnSe which proved to be very detrimental to the performance of CZTSe solar cells.[7]

ZnSe is observed as a segregated phase at the back of CZTSe absorbers,[8–10] as networks of nm-sized inclusions,[11] and as a layer on the top of the absorber.[7]

Since the usual lab methods, i.e., XRD[12] and green excitation Raman, are unable to detect ZnSe on CZTSe, as we demonstrate in this paper, we introduce green excitation Room Temperature Photoluminescence (RT-PL) as a non-destructive method to detect ZnSe in CZTSe.

CZTSe absorbers have been deposited on molybdenum coated soda lime glass by a precursor-annealing process. All samples were annealed in a tube furnace with Se and SnSe powders to prevent the decomposition of kesterite.[13] Precursors were prepared by two methods: co-evaporation or electroplating of stacked metals. Sample A is prepared by sequential potentiostatic electrodeposition of the metals (Cu/Sn/Zn) onto 2.5×2.5 cm^2 Mo coated glass substrates using a three-electrode setup with a platinum counter electrode, a reference electrode (saturated Hg/Hg_2Cl_2 for Cu deposition and Ag/AgCl for Sn and Zn), and a rotating disk electrode as working electrode, with a method adapted from Ref. 14. The potentials employed were −1.07 V (vs saturated Hg/Hg_2Cl_2), −0.75 V (vs Ag/AgCl), and −1.15 V (vs Ag/AgCl) for Cu, Sn, and Zn, respectively. The aqueous electroplating solutions contained 0.1M $CuSO_4$ for the deposition of Cu, 50 mM Sn(II) methanesulfonate for the deposition of tin, and 50 mM $ZnCl_2$ for the deposition of zinc. The finished absorber of sample A has a conversion efficiency of 2.1%. The method has led so far to a conversion efficiency of 5.5%, but we chose here a particularly Zn-rich sample. For sample B, the Cu, Zn, Sn, and Se elements are co-evaporated in a molecular beam epitaxy system at 320 °C.

This sample is resulting from a Cu rich ($Cu/Zn + Sn > 1$) precursor, which was KCN etched prior to annealing. Details of this so called "Capri" Process are found in the paper of Mousel *et al.*[15] The results shown in this publication are observed for a variety of annealing processes and etchings. The finished solar cell from sample B has a conversion efficiency of 6.2% and is exactly the same absorber as discussed in Ref. 11.

Raman and photoluminescence measurements were made in the same confocal home-built setup at different laser excitation wavelengths of an argon ion laser, namely 514.5 nm and 457.9 nm. The setup is also equipped with a piezo table which allows for measurements in scanning mode. The spectra shown here are either integrated line scans or point measurements. Raman measurements were made at different depths in the absorber by sequential thinning of the layer by sputtering craters of different depths. The sputter damaged layer was removed by a 15 s etching in a 0.02M Br_2 methanol solution. The excitation spot size is estimated to be about 1 μm in diameter. The spectra shown are taken at about 3 mW excitation laser power.

The elemental composition is measured by energy dispersive X-ray spectroscopy (EDX) at 20 kV electron acceleration voltage.

Figure 1(a) shows the composition of samples A and B plotted in the ternary phase diagram, as obtained by EDX analysis. Based on the assumption that only ZnSe and CZTSe are present, sample A is very rich in ZnSe, namely 64 mol. %, while sample B contains 18 mol. % of ZnSe and

[a)]Electronic mail: Rabie.djemour@uni.lu.
[b)]Current address: Energy and Semiconductor Research Laboratory, Department of Physics, University of Oldenburg, Oldenburg, Germany.

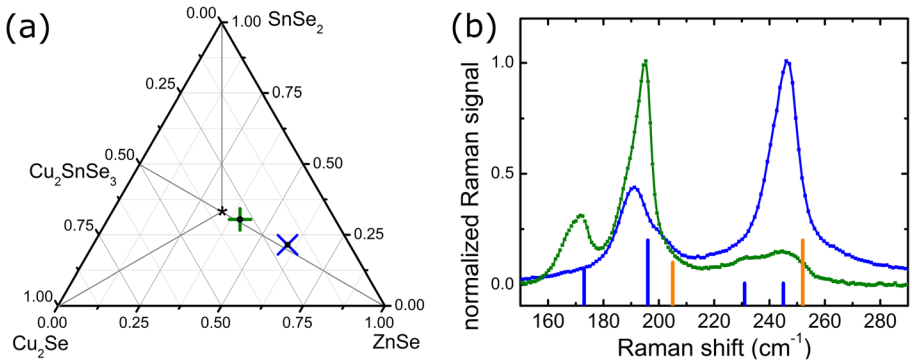

FIG. 1. (a) Ternary phase diagram showing composition of samples A(x) and B(+) (adapted from Ref. 3). (b) Normalized Raman spectra of sample A taken at 514.5 nm (shown in green; average spectrum of a 15 μm line scan) and 457.9 nm (shown in blue; single point measurement) excitation wavelengths. Reference peak positions for CZTSe (blue; see Ref. 16) and ZnSe (orange; see Ref. 17) are also included.

is grown in the composition area where record solar cells are grown.[16] Please note that in the case of sample A, EDX is likely to overestimate the ZnSe, because this phase segregates mostly on the surface for sample A. Figure 1(b) shows Raman spectra of sample A measured with two excitation wavelengths, namely 457.9 nm and 514.5 nm. These spectra are usually attributed to different materials: The green excitation Raman spectroscopy shows the spectrum of the pure CZTSe phase, while the blue excitation Raman shows the spectrum expected for ZnSe shifted by 5 cm^{-1}. This shift is explained by differences in strain and by the presence of impurities in the ZnSe. This emphasizes the difficulty of green excitation Raman spectroscopy to discern ZnSe when it coexists next to the CZTSe phase in the sample. The high sensitivity of the blue excitation to ZnSe is explained by the fact that the ZnSe is in preresonant condition for this excitation light. The green light is significantly below the photon energies, which are necessary for a quasi-resonant excitation and, therefore, is scattered with only a small Raman yield. Thus, it only can discern CZTSe, as long as the ZnSe is not a major phase in the layer (as shown by Ref. 18).

Figure 2 shows representative Raman and PL spectra taken on sample A. The green excitation photoluminescence shows a broad dominant transition at 1.3 eV and a second transition of lower intensity seen as a shoulder at about 0.9 eV. These two transitions occur at different relative intensities. The low energy transition is usually attributed to a CZTSe.[19] We will link the RT-PL luminescence peak at around 1.3 eV to a defect luminescence in ZnSe. This PL signal is at higher energy than the calculated[20] and measured[9,21] band gaps of CZTSe. It is also higher than the absorption edge observed in the quantum efficiency spectrum measured in solar cells made from this absorber. It is, therefore, attributed to a secondary phase of higher band gap. According to the composition of the samples and to the ternary phase diagram (Figure 1(a)), the most probable secondary phases are ZnSe, SnSe, and $SnSe_2$. SnSe and $SnSe_2$ can be excluded since these phases were not detected in green excitation Raman spectroscopy on the different samples. A thin layer of SnSe and $SnSe_2$ can be easily discerned in green excitation (514.5 nm) Raman spectroscopy as reported in Ref. 22. By exclusion, ZnSe is the only phase left to attribute this luminescence to, since this transition is seen with both green (2.41 eV; 514.5 nm) and blue (2.71 eV; 457.9 nm) excitation RT PL. In an earlier study, Redinger *et al.*[23] first proposed the attribution of this luminescence to ZnSe. In that paper, a PL band was presented, which could be attributed to the band-to-band transition of ZnSe. That was observed by UV excited photoluminescence,[23] supporting the attribution to ZnSe. Nevertheless, a direct proof of the ZnSe phase by a phase selective method was missing. The fact that in the current study we observe luminescence in ZnSe with an excitation energy lower than the band gap (514 nm, corresponding to 2.1 eV) is attributed to a highly defective ZnSe, which contains a high concentration of Cu and Sn impurities.[11] We assume that the excitation occurs via a defect related transition, while the luminescence is caused by another defect related transition. Different impurity related luminescences have already been observed far below the band gap in ZnSe.[24–26]

The proof that this luminescence is in fact a radiative transition in ZnSe is provided by the spatial correlation between the RT-PL and the blue excitation Raman spectroscopy signals. We discuss first the lateral correlation observed in sample A. The spectra shown in Figure 2 are from two points of the same 80×80 μm^2 scanned by green excitation PL and blue excitation Raman spectroscopy. The spectra shown in the same color are from the same points representative for areas with high (plotted in red) and low (plotted in black) 1.3 eV PL signal. The ZnSe contribution is dominating both the Raman and the PL spectra. In some cases, it is

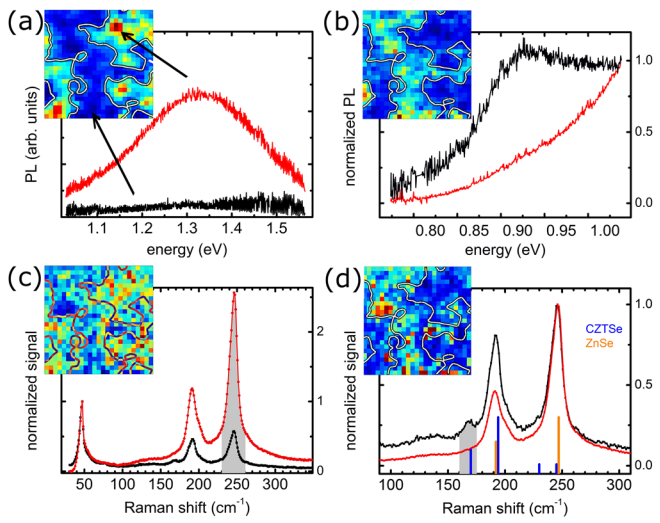

FIG. 2. Spectra of PL (514.5 nm excitation wavelength) ((a) and (b): different spectral ranges) and Raman (457.9 nm excitation wavelength) ((c) normalized to the reflected laser beam, (d) normalized to the main peak) from two representative points on sample A taken at room temperature. Insets show 80×80 μm^2 maps of spectrally integrated signals of the following energy ranges: (a) 1.0–1.6 eV (ZnSe), (b) 0.77–1.05 eV (CZTSe), (c) 230–260 cm^{-1}(ZnSe—shown in gray), and (d) 160–175 cm^{-1} (CZTSe—shown in gray). The intensities are given in arbitrary units with increasing intensity from blue over yellow to red. The contour from the inset of Figure 2(a) is plotted in the insets of Figures 2(b) to 2(d) as a guide to the eye.

necessary to normalize the PL and Raman data for each point of the mappings in order to deconvolute the small CZTSe-related signal from the ZnSe signal.

In Figure 2(a), we show the broad PL transition at 1.3 eV. For the related mappings, the as-measured intensity is integrated. In Figure 2(b), we show the normalized PL in the energy range 0.77 eV to 1.07 eV. In this spectral range, we expect the luminescence of the CZTSe, as discussed above. However, the signal height is strongly influenced by the peak tail of the emission at 1.3 eV. To remove this background, the intensity at 0.77 eV is set to zero and the intensity at 1.07 eV is set to 1. Thus, we normalize the contributions from the 1.3 eV peak and, therefore, highlight the CZTSe contribution under the assumptions that the CZTSe related PL is negligible at the borders of this energy range. The mapping shows the integrated intensity of the normalized spectra.

The Raman spectra from the same spots are shown in Figures 2(c) and 2(d) with different normalizations.

For both figures, the backgrounds are corrected by setting the high energy end of the spectrum to zero. In Figure 2(c), we normalize the rest of the reflected laser at 50 cm^{-1} to 1 to correct for different reflectivities at different points of the sample. The reflected laser is seen as a measurement artifact at 50 cm^{-1}. This is the incompletely removed part of the Rayleigh scattered laser light that is not cut off by the long pass edge filter. The mapping in Figure 2(c) shows this normalized intensity integrated from 230 to 260 cm^{-1}, i.e., in the spectral range of the main ZnSe mode. In order to better highlight the signal from CZTSe, the Raman signal shown in Figure 2(d) was normalized to the peak at 250 cm^{-1}, which is almost exclusively due to a ZnSe mode. This normalization shows the relative contribution of CZTSe compared to ZnSe when the peak at 170 cm^{-1} is integrated since this spectral range represents exclusively a CZTSe mode, with no contribution from ZnSe.

The insets in Figure 2 show the 80×80 m^2 maps of the RT-PL ((a) and (b)) and Raman ((c) and (d)) signals integrated in the energy ranges where the signal is dominated by either CZTSe or ZnSe. In order to highlight the correlation, one contour line from the RT-PL map (Figure 2(a)) is plotted in the other maps (Figures 2(b)–2(d)) as a guide to the eye. Comparison of the patterns in the maps indicates that the respective maps of ZnSe and CZTSe are anticorrelated, while the maps of ZnSe in PL (Figure 2(a)) and in Raman (Figure 2(c)) are correlated as well as the maps of CZTSe in PL (Figure 2(b)) and Raman (Figure 2(d)). To further corroborate the (anti) correlation of these signals, the Pearson product-moment correlation coefficient (PCC)[27] was computed. The PCCs are given in Table I. There is a strong anti-correlation of −0.8 between the two PL maps (representing the ZnSe and the CZTSe signal) as well as between the two Raman maps (representing the ZnSe and the CZTSe signal). This anti-correlation indicates that the areas with ZnSe and with CZTSe signal can be clearly separated in both maps. The (anti-) correlations between PL maps and Raman maps are considerably weaker, as is expected taking the different necessary normalizations into account. Still, there is significant correlation between the ZnSe PL map and the Raman map. This clearly shows that the PL signal at 1.3 eV is in fact due to a luminescent transition in ZnSe. The comparably low

TABLE I. PCC (see Ref. 27) for the integrated signals shown in the insets of Figure 2.

PCC	CZTSe PL (Fig. 2(b))	CZTSe Raman (Fig. 2(d))	ZnSe Raman (Fig. 2(c))
ZnSe PL (Fig. 2(a))	−0.76	−0.41	0.45
ZnSe Raman (Fig. 2(c))	−0.46	−0.79	
CZTSe Raman (Fig. 2(d))	0.34		

PCC of the Raman and PL signal of CZTSe of 0.34 is due to the fact that there is no energy range in either spectrum, which is purely due to a CZTSe signal. In fact, the background of the pure CZTSe Raman peak at 170 cm^{-1} is given by the peak at 190 cm^{-1} which has ZnSe and CZTSe components and the PL signal around 0.9 eV has a strong background from the broad 1.3 eV ZnSe peak.

This paragraph will show that ZnSe defect luminescence also correlates with the Raman signal as a function of depth of the film and that the RT-PL signature of ZnSe enables us to discern quite small amounts of ZnSe segregation in CZTSe. In Figure 3, the RT-PL spectrum of sample B (plotted in black) shows the expected PL peak from CZTSe at around 0.95 eV with a high energy shoulder that we attribute to ZnSe (fit shown in red, with a maximum at 1.2 eV). The blue graph in Figure 3 is a corrected "CZTSe only" spectrum obtained by subtracting the ZnSe shoulder peak from the measured spectrum. Figure 4 shows two Raman spectra taken at green and blue excitation wavelengths, similar to the spectra acquired for sample A (Figure 1). The main difference between the two samples is that the contribution from ZnSe is much lower in sample B. In fact, the ZnSe Raman signal is very low and never dominates the spectrum. Only the main mode at 250 cm^{-1} is seen when blue excitation is used. This peak also has contributions from CZTSe. Thus, the intensity ratio of the peaks at 250 cm^{-1} and 235 cm^{-1} is chosen to quantify the ZnSe content assuming a comparable peak height of the two CZTSe modes at 235^{-1} and 250 cm^{-1}.

In Figure 5, the ZnSe PL intensity and the ZnSe content acquired from the Raman peak ratio are plotted as a function of the depth of the film (sputter time varied to prepare the craters of different depth). There is a strong correlation between the two measurements that further strengthens the attribution of the PL signal at ∼1.25 eV to the ZnSe phase.

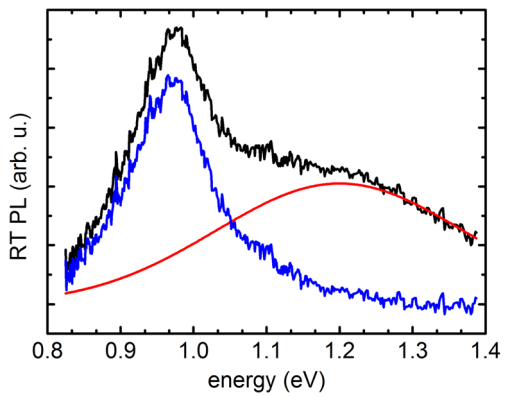

FIG. 3. Micro RT-PL spectrum taken on sample B (black). A fit of the luminescence attributed to Zn Se is shown in red. The rest spectrum, i.e., the signal related to CZTSe is shown in blue.

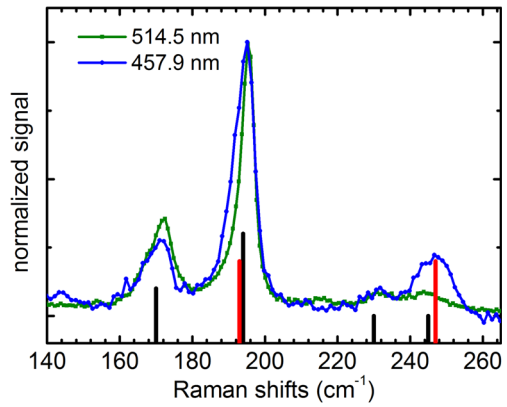

FIG. 4. Normalized micro Raman measurements taken at the same depth of sample B at different excitation wavelengths (green for 514.5 nm excitation, blue for 457.9 nm excitation). ZnSe (red) and CZTSe (black) peak positions are marked.

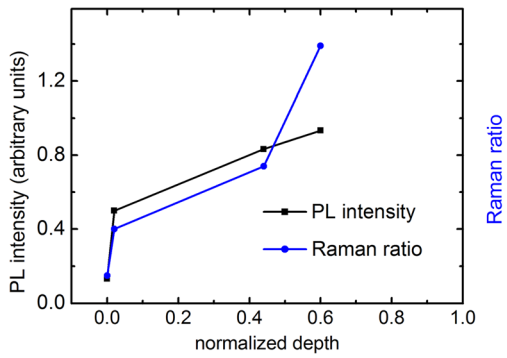

FIG. 5. Evolution PL (black) and Raman (blue) signal intensities as a function of depth. For the Raman peak intensity, the ratio of the intensities ($I(250\,cm^{-1})$–$I(235\,cm^{-1})$)/$I(235\,cm^{-1})$ is plotted.

This broad luminescence is observed at different energy positions in the range of 1.20–1.32 eV as can be seen by comparing the peak positions reported in Refs. 22 and 23 and in Figures 2(a) and 3 of this study. This variation is attributed to different doping or impurity concentrations and/or doping materials, e.g., Cu and/or Sn as seen in the atom probe tomographies (APTs) performed on sample B.[11] These APT measurements showed nm sized ZnSe networks with copper and tin impurities of up to 3 at. %. The detection of such small islands of secondary phase proves the power of this technique.

To conclude, we confirmed that green excitation standard Raman spectroscopy is not sufficient to detect the co-existing ZnSe secondary phase in CZTSe; blue excitation is necessary for quasi-resonant Raman. The RT-PL emission at 1.20–1.32 eV could be clearly correlated to a defect luminescence of ZnSe by spatially correlating this PL emission to the known Raman signal of ZnSe. We finally show the sensitivity of this simple technique (i.e., RT-PL) for the detection of comparatively small amounts of the ZnSe secondary phase.

The authors acknowledge the financial support by the Luxembourgish Fonds National de la Recherche and the EU seventh framework programme FP7/2007-2013 under Grant No. 284486, and the use of the SEM apparatus through the CRP Lippmann (Luxembourg). The authors would like to thank Nathalie Valle for the sputtering of the craters needed for the depth resolution.

[1]I. Repins, C. Beall, N. Vora, C. DeHart, D. Kuciauskas, P. Dippo, B. To, J. Mann, W. C. Hsu, A. Goodrich, and R. Noufi, Sol. Energy Mater. Sol. Cells **101**, 154–159 (2012).
[2]I. Dudchak and L. Piskach, J. Alloys Compd. **351**(1), 145–150 (2003).
[3]S. Chen, X. G. Gong, A. Walsh, and S.-H. Wei, Phys. Rev. B **79**(16), 165211 (2009).
[4]C. Persson, J. Appl. Phys. **107**(5), 053710 (2010).
[5]B. Shin, O. Gunawan, Y. Zhu, N. A. Bojarczuk, S. J. Chey, and S. Guha, Prog. Photovoltaics **21**(1), 72–76 (2013).
[6]S. Siebentritt, Thin Solid Films **535**, 1–4 (2013).
[7]J. T. Watjen, J. Engman, M. Edoff, and C. Platzer-Bjorkman, Appl. Phys. Lett. **100**(17), 173510 (2012).
[8]J. J. Scragg, J. T. Wätjen, M. Edoff, T. Ericson, T. Kubart, and C. Platzer-Björkman, J. Am. Chem. Society **134**(47), 19330–19333 (2012).
[9]S. Ahn, S. Jung, J. Gwak, A. Cho, K. Shin, K. Yoon, D. Park, H. Cheong, and J. H. Yun, Appl. Phys. Lett. **97**(2), 021905 (2010).
[10]A. Redinger, K. Hoenes, X. Fontané, V. Izquierdo-Roca, E. Saucedo, N. Valle, A. Pérez Rodríguez, and S. Siebentritt, Appl. Phys. Lett. **98**(10), 101907 (2011).
[11]T. Schwarz, O. Cojocaru-Mirédin, P. Choi, M. Mousel, A. Redinger, S. Siebentritt, and D. Raabe, Appl. Phys. Lett. **102**(4), 042101–042104 (2013).
[12]O. Volobujeva, J. Raudoja, E. Mellikov, M. Grossberg, S. Bereznev, and R. Traksmaa, J. Phys. Chem. Solids **70**(3–4), 567–570 (2009).
[13]A. Redinger, D. M. Berg, P. J. Dale, and S. Siebentritt, J. Am. Chem. Soc. **133**(10), 3320–3323 (2011).
[14]J. J. Scragg, D. M. Berg, and P. J. Dale, J. Electroanal. Chem. **646**(1–2), 52–59 (2010).
[15]M. Mousel, T. Schwarz, R. Djemour, T. P. Weiss, A. Redinger, O. Cojocaru-Miredin, P. Choi, and S. Siebentritt "Cu-rich precursors improve kesterite solar cells," Adv. Energy Mater. (submitted).
[16]M. Grossberg, J. Krustok, K. Timmo, and M. Altosaar, Thin Solid Films **517**(7), 2489–2492 (2009).
[17]N. Vora, J. Blackburn, I. Repins, C. Beall, B. To, J. Pankow, G. Teeter, M. Young, and R. Noufi, J. Vac. Sci. Technol. A **30**(5), 051201 (2012).
[18]A. Fairbrother, E. Saucedo, X. Fontané, V. Izquierdo-Roca, D. Sylla, M. Espindola-Rodriguez, F. Pulgarin-Agudelo, O. Vigil-Galan, and A. Pérez Rodríguez, paper presented at the 38th IEEE Photovoltaic Specialists Conference (PVSC), 2012.
[19]E. Mellikov, M. Altosaar, M. Krunks, J. Krustok, T. Varema, O. Volobujeva, M. Grossberg, L. Kaupmees, T. Dedova, K. Timmo, K. Ernits, J. Kois, I. O. Acik, M. Danilson, and S. Bereznev, Thin Solid Films **516**(20), 7125–7134 (2008).
[20]S. Chen, A. Walsh, J.-H. Yang, X. G. Gong, L. Sun, P.-X. Yang, J.-H. Chu, and S.-H. Wei, Phys. Rev. B **83**(12), 125201 (2011).
[21]S. Bag, O. Gunawan, T. Gokmen, Y. Zhu, T. K. Todorov, and D. B. Mitzi, Energy Environ. Sci. **5**(5), 7060–7065 (2012).
[22]A. Redinger, M. Mousel, R. Djemour, L. Gütay, N. Valle, and S. Siebentritt, "$Cu_2ZnSnSe_4$ thin film solar cells produced via co-evaporation and annealing including a $SnSe_2$ capping layer," Prog. Photovoltaics DOI:10.1002/pip.2324 (published online).
[23]A. Redinger, D. M. Berg, P. J. Dale, R. Djemour, L. Gütay, T. Eisenbarth, N. Valle, and S. Siebentritt, IEEE J. Photovoltaics **1**(2), 200–206 (2011).
[24]G. B. Stringfellow and R. H. Bube, Phys. Rev. **171**(3), 903–915 (1968).
[25]N. K. Morozova, I. A. Karetnikov, V. V. Blinov, and E. M. Gavrishchuk, Semiconductors **35**(5), 512–515 (2001).
[26]N. K. Morozova, I. A. Karetnikov, V. V. Blinov, and E. M. Gavrishchuk, Semiconductors **35**(1), 24–32 (2001).
[27]J. L. Rodgers and W. A. Nicewander, Am. Stat. **42**(1), 59–66 (1988).